THE JOURNAL OF PHYSICAL CHEMISTRY A
A JOURNAL OF THE AMERICAN CHEMICAL SOCIETY

pubs.acs.org/JPCA

Article

Electronic *g*-Tensor Calculations for Dangling Bonds in Nanodiamonds

Šarūnas Masys,* Valdas Jonauskas, and Zilvinas Rinkevicius

Cite This: https://doi.org/10.1021/acs.jpca.1c06253

Read Online

ACCESS | Metrics & More | Article Recommendations

ABSTRACT: The electronic *g*-tensor calculations are performed for dangling bonds (DBs) introduced into nanodiamonds (NDs) with four different functional groups on their surfaces. For hydrogenated and fluorinated NDs, it is found that *g*-shifts of the latter vary in a much wider range, and the same is also true for the total energy differences between the highest and the lowest energy DBs. In addition, it is shown that the shape of NDs significantly impacts the energetics and *g*-shifts of DBs, whereas the influence of the size is much less pronounced, as is the influence of the presence of one DB in the vicinity of the other, resulting in no substantial change on their magnetic behavior. For hydroxylated and aminated NDs, it is demonstrated that the variation range of *g*-shifts is larger for the former, whereas the opposite is seen regarding the total energy differences. On the whole, some of the positions of DBs can be energetically very costly in these NDs; besides, the lowest energy DBs are irregular, that is, formed by OH- and NH_2-bonded C atoms, contrasting with hydrogenated and fluorinated NDs, for which irregular DBs are the most energetically unfavorable.

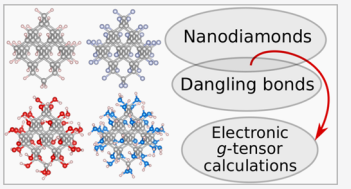

INTRODUCTION

Nanodiamonds (NDs), being well suited to act as theranostic platforms,[1−3] deserve special attention among the members of the vast family of biotechnologically attractive nanoparticles.[4] In recent years, biomedical applications of NDs have become even more promising due to the experimental findings that, along with luminescence-based techniques, NDs can also be directly[5] or indirectly[6] detected using magnetic resonance imaging (MRI)—the gold standard for non-invasive high-contrast visualization. Within the MRI framework, the direct detection of ND is performed *via* its ^{13}C nuclei, while the imaging of ^{1}H nuclei surrounding the ND is required for its indirect detection. However, neither of these MRI scans for NDs would be successful without the presence of paramagnetic centers, the suitable reservoir of which is necessary for the transfer of spin polarization from their electrons to the aforementioned carbon and hydrogen nuclei. Luckily, electron paramagnetic resonance (EPR) measurements have shown[1,5,6] that commercially available high-pressure high-temperature NDs provide such a reservoir, most likely in the form of surface dangling bonds (DBs) and other paramagnetic impurities. As carbon DBs of sp^3-type are considered one of the most abundant paramagnetic defects in NDs,[7,8] they have become the focus of our research.

Unlike other spectroscopic and analytical methods, EPR is able to offer important information about the structure and dynamics of a system, including the chemical and physical processes occurring therein.[8] Since electronic *g*-tensor, describing the magnetic moments of the unpaired electrons under the influence of their local environment,[9] is one of the key parameters of this powerful tool, its careful analysis is crucial for the proper interpretation of the measured EPR spectra. Therefore, we have carried out *g*-tensor calculations for DBs introduced into NDs with experimentally realized or even commercially available surfaces consisting of such groups[10] as H, F, OH, and NH_2—similarly as in the study on magnetical and optical properties of nitrogen vacancy centers.[11] Concerning hydrogenated NDs, we have expanded our previous work[12] by including octahedrally shaped $C_{165}H_{100}$ among the modeled systems, while for fluorinated NDs, octahedral $C_{84}F_{64}$ and $C_{165}F_{100}$, as well as cubic $C_{54}F_{48}$ and tetrahedral $C_{51}F_{52}$, were newly added. Hydroxylated and aminated NDs were fully investigated for the first time, but due to the substantially increased amount of calculations, we have confined ourselves to the smallest models $C_{35}(OH)_{36}$ and $C_{35}(NH_2)_{36}$ of the most common octahedral shape.[13] In addition, the simultaneous presence of several DBs in hydrogenated and fluorinated NDs was analyzed and a comparison of the obtained results to the available experimental data was presented. Overall, this type of investigation not only allowed us to produce new information on the *g*-tensor values but also provided interesting insights into the formation of DBs from the energetic point of view and their identification in EPR spectra.

Received: July 13, 2021

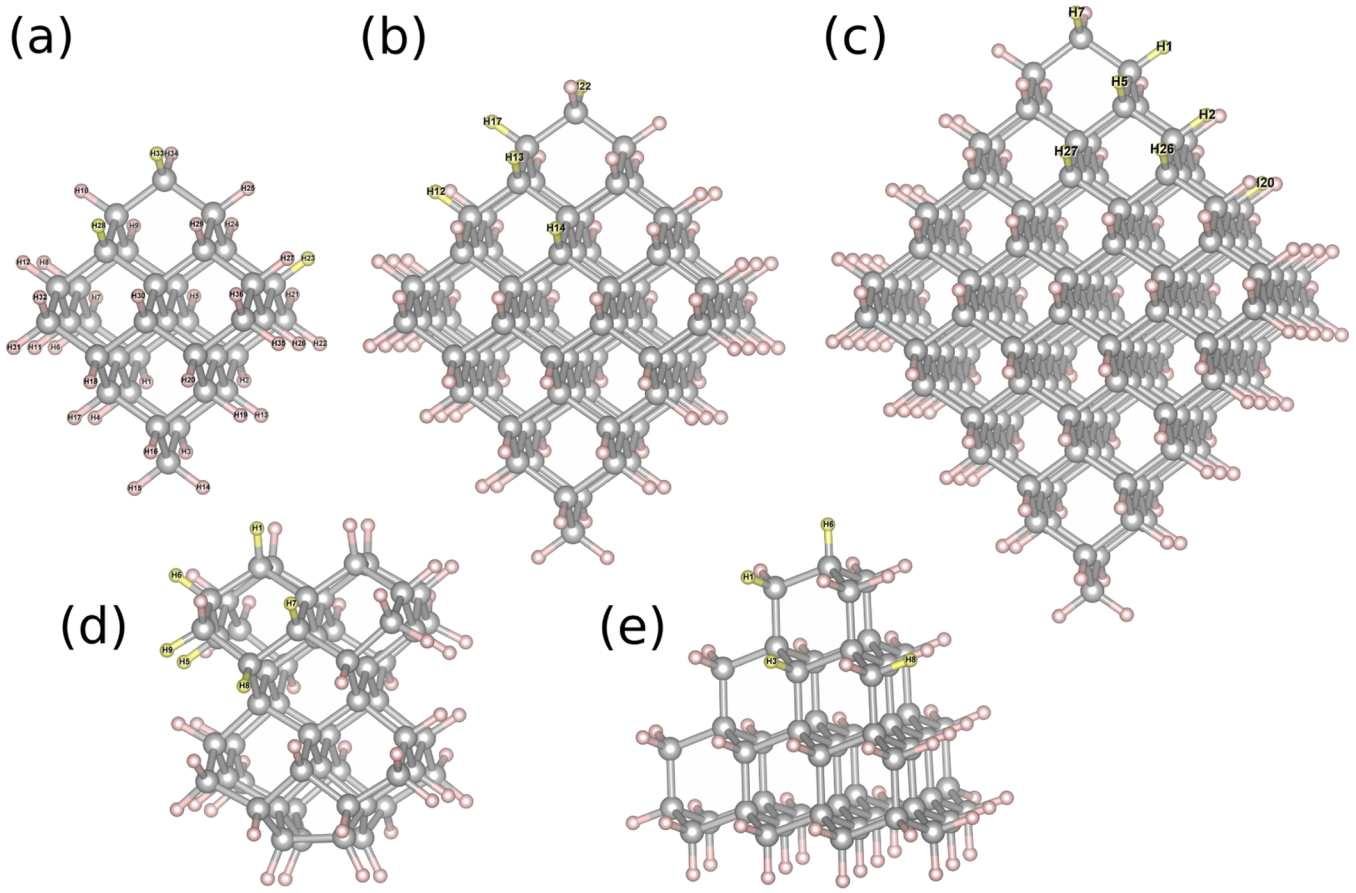

Figure 1. Visual representation of hydrogenated NDs: octahedrally shaped (a) $C_{35}H_{36}$, (b) $C_{84}H_{64}$, and (c) $C_{165}H_{100}$, as well as (d) cubic $C_{54}H_{48}$ and (e) tetrahedral $C_{51}H_{52}$. Gray and pink balls stand for carbon and hydrogen atoms, respectively. The numbered hydrogen atoms, colored in yellow, were used for modeling DBs.

COMPUTATIONAL DETAILS

All results presented in this study were obtained using the ORCA (version 4.2.1) quantum chemistry package.[14,15] For the geometry optimization, a low-cost PBEh-3c method,[16] applied in our recent work on the hydrophilic and hydrophobic NDs interacting with water,[17] was chosen, while for the *g*-tensor calculations, a combination of hybrid B3LYP functional[18,19] and 6-311G(2d,2p) basis set,[20,21] tested in our previous investigation on the magnetic properties of NDs,[22] was utilized.

The default values were selected for most of the technical setup; however, DFT integration grid for the self-consistent field (SCF) procedure was increased (keyword GRID7), whereas grid for the final energy evaluation was turned off. Additionally, tight convergence criteria were set for geometry optimization and SCF procedure in the case of PBEh-3c calculations and very tight convergence criteria were chosen for SCF procedure in the case of B3LYP/6-311G(2d,2p) calculations. For the latter combination, modified resolution of the identity (RI)[23] and chain of sphere (COS)[24] techniques, commonly known as RIJCOSX approximation, were correspondingly adopted for the Coulomb and Hartree−Fock (HF) exchange interactions. An auxiliary Coulomb-fitting basis set was generated automatically.[25] For the sake of greater accuracy while exploiting the gauge-including atomic orbitals within the effective nuclear charge framework,[26−28] default COS grid was strongly tightened (keywords GRIDX9), with the final one being turned off. On the other hand, only RI technique with an auxiliary def2/J basis set[29] was applied for the PBEh-3c method, as HF exchange interaction was treated in full. Moreover, the basis set superposition error and long-range London dispersion effects were taken into account through atom-pairwise geometrical counter-poise[30] and D3 dispersion (with Becke−Johnson damping)[31,32] correction schemes, respectively. In order to evaluate some additional hyperfine coupling constants, we have utilized the same parameters as in the case of *g*-tensor calculations, except for the basis set, which was changed to EPR-II,[33] since it enables a better description of the spin density near nuclei.

DBs were introduced into NDs by removing appropriate H, F, OH, or NH_2 atoms. Thus, notation DB(X) indicates that atom(s) X (their position can be found in figures) were removed from the system. All figures were produced using the visualization program VESTA[34] with the isovalues of the spin density isosurfaces set to 0.0075 e/a_0^3 (see Figures 3 and 4). The results of the *g*-tensor calculations were mainly presented in the form of *g*-shifts Δg_{ii} ($i = x, y, z$), which were obtained by subtracting the free electron *g*-factor ($g_e = 2.0023193$) from the positive square roots of the eigenvalues of $g^T \cdot g$, with g denoting the *g*-tensor. Moreover, the *g*-shifts were given in such an order that $\Delta g_{xx} < \Delta g_{yy} < \Delta g_{zz}$. Their isotropic values $\Delta\bar{g}$ were taken as an arithmetic average of Δg_{ii}.

In our previous paper on *g*-tensor dependence on the size, shape, and surface functionalization of NDs,[12] geometry optimization and *g*-tensor calculations were carried out using the same B3LYP/cc-pVTZ framework. Here, some of the

https://doi.org/10.1021/acs.jpca.1c06253
J. Phys. Chem. A XXXX, XXX, XXX−XXX

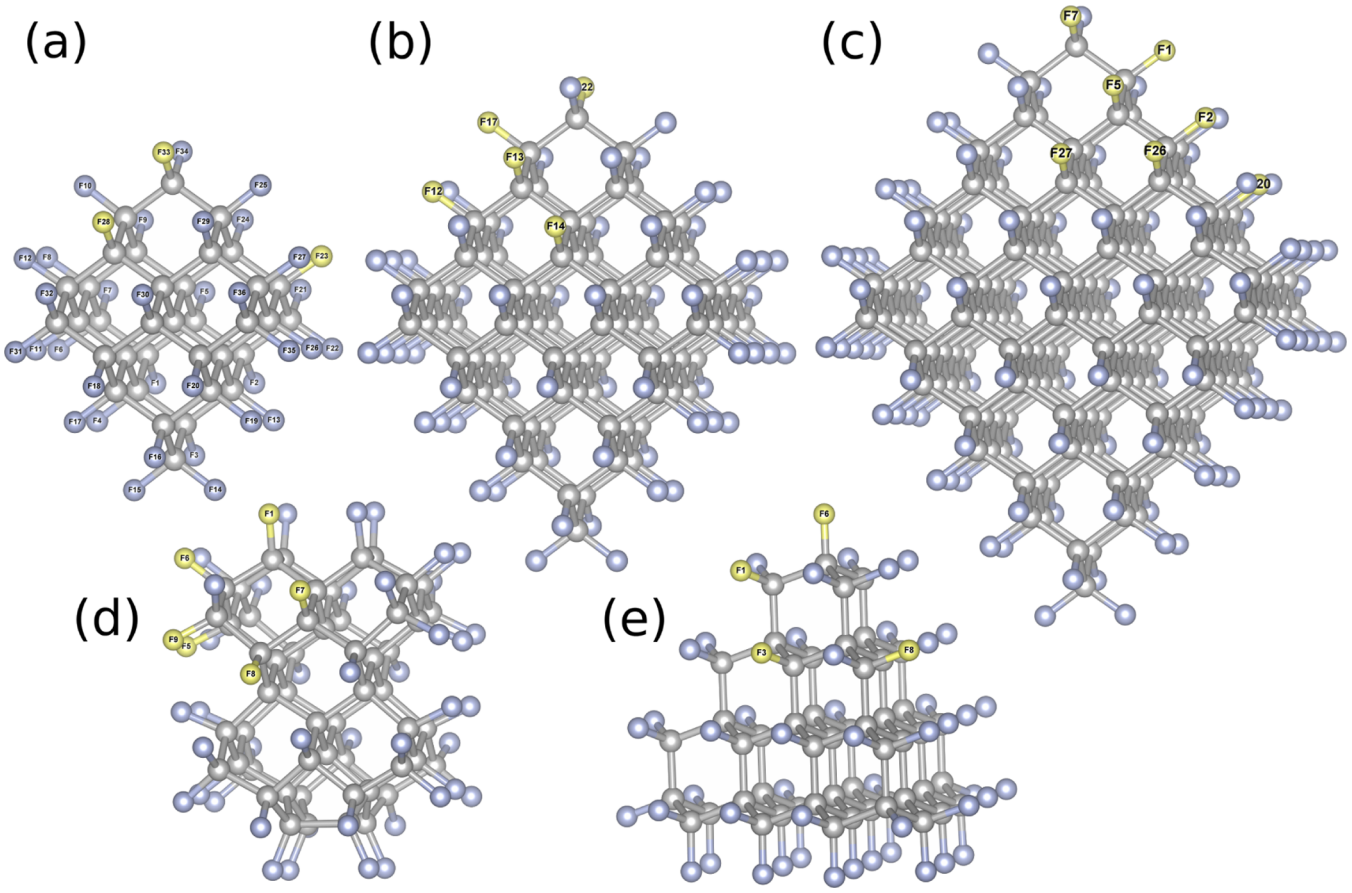

Figure 2. Visual representation of fluorinated NDs: octahedrally shaped (a) $C_{35}F_{36}$, (b) $C_{84}F_{64}$, and (c) $C_{165}F_{100}$ as well as (d) cubic $C_{54}F_{48}$ and (e) tetrahedral $C_{51}F_{52}$. Gray and blue balls stand for carbon and fluorine atoms, respectively. The numbered fluorine atoms, colored in yellow, were used for modeling DBs.

calculations were intentionally repeated in order to assess the performance of a combined PBEh-3c and B3LYP/6-311G(2d,2p) scheme. A comparison between the average values of $\Delta\overline{g}$ for $C_{35}H_{36}$, $C_{84}H_{64}$, $C_{54}H_{48}$, $C_{51}H_{52}$, and $C_{35}F_{36}$ shows that the difference between previous and current results does not correspondingly exceed 5, 5, 7, 4, and 24 parts per million (ppm). Having in mind that the experimental precision of recent EPR measurements for NDs can be limited to 200 ppm,[7] such a good agreement clearly indicates that our current results are of the same quality as the ones obtained employing full triple-ζ basis set with *d* polarization function for H and *f* polarization function for the rest of the atoms. However, the obvious advantage of PBEh-3c and B3LYP/6-311G(2d,2p) combination is a significantly reduced computational cost, which becomes particularly important when a number of calculations increases and/or systems under consideration get larger.

RESULTS AND DISCUSSION

Hydrogenated and Fluorinated NDs. In order to reduce the effort to obtain a set of *g*-tensors that would fully describe this type of magnetic behavior in hydrogenated and fluorinated NDs with introduced DBs, it is highly beneficial to exploit the symmetry they possess. As we have already discussed previously,[12,22] the existence of geometrically and, therefore, energetically equivalent positions of H and F atoms allows one to consider only four DBs in tetrahedral, six DBs in cubic, and from three to seven DBs in octahedral NDs. The H and F atoms that were used for modeling DBs are visualized in Figures 1 and 2, respectively. The corresponding results of *g*-tensor calculations together with total energy differences are provided in Tables 1 and 2.

Regarding hydrogenated NDs of octahedral shape, it can be noted that despite various sizes, the isotropic values of *g*-shifts fall in an almost identical range: from 326 to 436 ppm for $C_{35}H_{36}$, from 323 to 460 ppm for $C_{84}H_{64}$, and from 324 to 466 ppm for $C_{165}H_{100}$. Such a close resemblance suggests that a further increase in size most probably will give similar results. However, it is interesting to observe that for all octahedral NDs, the lowest $\Delta\overline{g}$ values are shown by H-bonded dangling C atoms, that is, DBs formed by removing one of two H atoms attached to a single C atom. To be concrete, these are DB(H33), DB(H22), and DB(H7) for $C_{35}H_{36}$, $C_{84}H_{64}$, and $C_{165}H_{100}$, respectively. It is also worth mentioning that these DBs are obviously the least energetically favorable in comparison to regular DBs possessing no H atoms.

The situation is slightly different for tetrahedral ND. Although the lowest $\Delta\overline{g}$ values of 301 and 303 ppm still belong to H-bonded dangling C atoms [DB(H1) and DB(H8)], their energies are similar to that of a regular DB [DB(H3)], and they all are above the lowest energy DB [DB(H6)] by ∼1 kcal/mol. Interestingly, the situation is even more different for cubic ND since not only its H-bonded dangling C atom [DB(H9)] has the energy that is very close to that of the lowest energy DB [DB(H8)] but also the isotropic value of *g*-shifts (454 ppm) is also higher than those of other

https://doi.org/10.1021/acs.jpca.1c06253
J. Phys. Chem. A XXXX, XXX, XXX−XXX

Table 1. *g*-Shifts Δg_{ii} and Their Isotropic Values $\Delta\bar{g}$ (in ppm) Calculated for DBs Introduced into Hydrogenated NDs of Different Sizes and Shapes[a]

hydrogenated ND	DB position	N	Δg_{xx}	Δg_{yy}	Δg_{zz}	$\Delta\bar{g}$	ΔE
octahedral $C_{35}H_{36}$	H33	12	40	143	795	326	0.70
	H28	12	−90	661	676	416	0.43
	H23	12	−100	617	791	436	
octahedral $C_{84}H_{64}$	H22	12	45	128	796	323	0.82
	H13	24	−78	618	738	426	0.34
	H14	4	−59	681	682	435	0.33
	H17	12	−99	610	799	436	0.17
	H12	12	−66	702	743	460	
octahedral $C_{165}H_{100}$	H7	12	48	124	799	324	0.73
	H5	24	−77	612	752	429	0.27
	H1	12	−99	608	805	438	0.09
	H27	12	−59	675	703	440	0.35
	H20	4	−55	699	699	448	0.29
	H2	24	−65	704	756	465	
	H26	12	−66	722	742	466	0.08
cubic $C_{54}H_{48}$	H1	8	−156	395	686	308	6.47
	H5	4	−90	285	755	317	3.11
	H9	16	49	388	924	454	0.18
	H6	8	−104	749	877	507	0.73
	H8	8	−110	796	868	518	
	H7	4	−79	722	987	543	0.31
tetrahedral $C_{51}H_{52}$	H1	24	−24	186	741	301	1.14
	H8	12	31	157	722	303	0.96
	H3	12	−52	664	687	433	0.99
	H6	4	−119	834	834	517	

[a]The number of geometrically equivalent DBs in a given ND is denoted by N, while ΔE represents the total energy difference (in kcal/mol) of DBs with respect to the lowest energy DB.

Table 2. *g*-Shifts Δg_{ii} and Their Isotropic Values $\Delta\bar{g}$ (in ppm) Calculated for DBs Introduced into Fluorinated NDs of Different Sizes and Shapes[a]

fluorinated ND	DB position	N	Δg_{xx}	Δg_{yy}	Δg_{zz}	$\Delta\bar{g}$	ΔE
octahedral $C_{35}F_{36}$	F23	12	−477	97	518	46	3.17
	F28	12	−160	602	838	427	
	F33	12	−363	2356	3026	1673	4.45
octahedral $C_{84}F_{64}$	F17	12	−386	272	669	185	4.51
	F12	12	−214	302	858	316	2.49
	F13	24	−108	573	1126	530	1.66
	F14	4	−6	888	888	590	
	F22	12	−338	2404	3001	1689	6.08
octahedral $C_{165}F_{100}$	F1	12	−373	304	693	208	4.99
	F2	24	−134	388	1029	428	2.58
	F26	12	−77	468	1102	498	2.10
	F5	24	−90	590	1206	569	2.14
	F20	4	34	1017	1017	689	0.38
	F27	12	59	1058	1069	729	
	F7	12	−330	2418	2994	1694	6.62
cubic $C_{54}F_{48}$	F6	8	−504	−70	465	−36	8.56
	F5	4	−346	234	271	53	
	F1	8	−311	241	421	117	15.09
	F7	4	−264	166	640	181	2.79
	F8	8	−172	117	670	205	0.11
	F9	16	−230	2268	2883	1640	9.09
tetrahedral $C_{51}F_{52}$	F6	4	−395	−380	−380	−385	8.95
	F3	12	195	894	1361	817	
	F1	24	−144	2639	3151	1882	6.19
	F8	12	−90	2850	3134	1965	4.64

[a]The number of geometrically equivalent DBs in a given ND is denoted by N, while ΔE represents the total energy difference (in kcal/mol) of DBs with respect to the lowest energy DB.

https://doi.org/10.1021/acs.jpca.1c06253
J. Phys. Chem. A XXXX, XXX, XXX−XXX

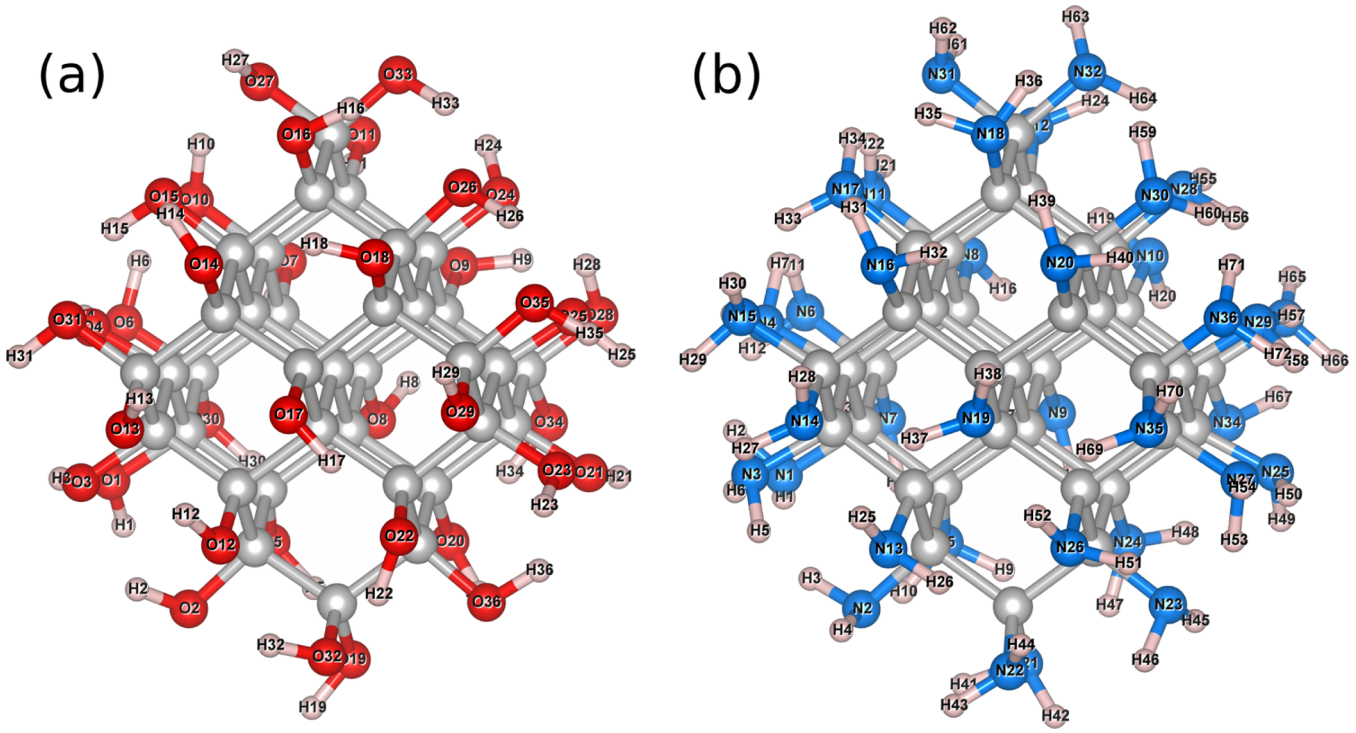

Figure 3. Visual representation of octahedrally shaped (a) hydroxylated and (b) aminated NDs of $C_{35}(OH)_{36}$ and $C_{35}(NH_2)_{36}$ size, respectively. Gray, pink, red, and azure balls correspondingly stand for carbon, hydrogen, oxygen, and nitrogen atoms.

regular DBs, that is, DB(H1) with 308 ppm and DB(H8) with 317 ppm. Concerning the latter DBs, they are definitely the most energetically unfavorable, as their total energy differences correspondingly reach 6.47 and 3.11 kcal/mol. These numbers are far above the ones demonstrated by octahedral (0.82 kcal/mol of $C_{84}H_{64}$) and tetrahedral (1.14 kcal/mol) NDs, pointing to the fact that the shape plays an important role on the energetics of DBs embedded into NDs.

In contrast to hydrogenated NDs for which $\Delta\bar{g}$ values vary in a quite narrow range of 242 ppm (from 301 to 543 ppm), fluorinated NDs exhibit a significantly larger variation of 2350 ppm (from −385 to 1965 ppm), seen in Table 2. The same tendency can also be noticed for the total energy differences, indicating that the local environment created by F atoms has a much more pronounced impact on the energetics as well as magnetic properties of the investigated systems. Speaking about octahedral NDs, the ranges of their isotropic *g*-shifts are not too different from one another: from 46 to 1673 ppm for $C_{35}F_{36}$, from 185 to 1689 ppm for $C_{84}F_{64}$, and from 208 to 1694 ppm for $C_{165}F_{100}$. This observation is in agreement with the trend inherent for hydrogenated NDs, as is the fact that F-bonded dangling C atoms—DB(F33), DB(F22), and DB(F7)—are the least energetically favorable among all DBs available in a particular ND. However, now their $\Delta\bar{g}$ values are not the lowest but the highest ones. In addition, unlike in hydrogenated NDs, this tendency also holds for the rest of NDs since DB(F1) and DB(F8) of tetrahedral ND and DB(F9) of cubic ND have $\Delta\bar{g}$ of 1882, 1965, and 1640 ppm, respectively. On the other hand, the energies of these DBs are neither the highest nor the lowest ones, similarly as in hydrogenated NDs. On the whole, F-bonded dangling C atoms appear to be truly special regarding $\Delta\bar{g}$ values, as they are at least ∼1000 ppm larger compared to those of regular DBs, irrespective of the shape and size of NDs. Concerning tetrahedral NDs, the variation range of its $\Delta\bar{g}$ values (2350 ppm) is substantially larger than the corresponding variation ranges of octahedral (1627 ppm of $C_{35}F_{36}$) and cubic (1676 ppm) NDs, allowing to state that the shape is an important factor not only for the energetics but also for the *g*-shifts in such systems.

One of the most interesting observations that can be made while examining the results of hydrogenated and fluorinated NDs is related with the lowest energy DBs, which, surprisingly enough, does not coincide. To be precise, not a single geometric position of the lowest energy DB in hydrogenated ND matches the same geometric position of the lowest energy DB in fluorinated NDs, indicating that how differently these geometrically identical systems behave. Just to confirm this diversity, it can be noted that for tetrahedral NDs, a geometric position of the lowest energy DB in $C_{51}H_{52}$ [DB(H6)] turns out to be a geometric position of the highest energy DB in $C_{51}F_{52}$ [DB(F6)]. However, on the other hand, there are some nice coincidences in the case of the highest energy DBs. In addition to the aforementioned octahedral NDs, the energetic behavior of the highest energy DBs in cubic systems is very similar too, as DB(H1) and DB(F1) are clearly the most energetically unfavorable DBs among all.

Hydroxylated and Aminated NDs. From a geometric point of view, the situation with hydroxylated and aminated NDs is quite different in comparison to hydrogenated and fluorinated NDs. The reason for this is that these systems possess more degrees of freedom due to the presence of spatially more complicated surface structure. It basically indicates that in order to obtain a set of *g*-tensors that would provide a full view of this type of magnetic behavior, one should perform calculations for all possible DBs since, strictly speaking, geometrically equivalent DBs no longer exist. Having that in mind, we have confined ourselves to the smallest

https://doi.org/10.1021/acs.jpca.1c06253
J. Phys. Chem. A XXXX, XXX, XXX−XXX

models of octahedral shape, that is, $C_{35}(OH)_{36}$ and $C_{35}(NH_2)_{36}$, to make the investigation feasible with computational resources available to us. The visual representation of $C_{35}(OH)_{36}$ and $C_{35}(NH_2)_{36}$ can be found in Figure 3, whereas the results of *g*-tensor calculations together with total energy differences are given in Tables 3 and 4, respectively.

Table 3. *g*-Shifts Δg_{ii} and Their Isotropic Values $\Delta\bar{g}$ (in ppm) Calculated for DBs Introduced into Hydroxylated Octahedral NDs of $C_{35}(OH)_{36}$ Size[a]

DB position	Δg_{xx}	Δg_{yy}	Δg_{zz}	$\Delta\bar{g}$	ΔE
O2−H2	−360	163	461	88	13.2
O18−H18	−370	211	530	124	16.5
O16−H16	−275	211	449	128	14.5
O3−H3	−315	198	524	135	12.2
O11−H11	−303	105	636	146	14.9
O7−H7	−298	224	577	168	12.4
O36−H36	−316	161	666	170	15.5
O21−H21	−329	290	553	171	12.0
O23−H23	−325	280	559	171	17.2
O14−H14	−269	240	588	186	13.8
O9−H9	−291	276	599	195	12.3
O1−H1	−267	285	688	236	12.5
O26−H26	−213	446	819	351	12.5
O4−H4	−103	520	768	395	7.0
O22−H22	−124	535	779	397	9.4
O20−H20	−143	475	894	409	5.0
O5−H5	−159	524	880	415	8.0
O25−H25	−119	456	922	420	4.0
O15−H15	−123	546	845	423	8.2
O17−H17	−111	561	858	436	8.9
O8−H8	−115	477	947	436	7.2
O24−H24	−88	537	924	458	10.4
O12−H12	−86	576	917	469	6.9
O10−H10	−68	575	954	487	10.9
O34−H34	−177	1023	1143	663	13.0
O33−H33	−232	1074	1981	941	6.0
O28−H28	−294	1125	2011	948	10.1
O6−H6	−280	1176	2148	1015	5.0
O29−H29	−246	1155	2142	1017	6.0
O32−H32	−238	1225	2085	1024	2.7
O31−H31	−245	1180	2160	1032	1.1
O13−H13	−234	1183	2183	1044	1.6
O30−H30	−254	1223	2164	1044	1.8
O35−H35	−234	1258	2121	1048	
O27−H27	−227	1348	2191	1104	6.4
O19−H19	−231	1304	2265	1113	3.2

[a]ΔE represents the total energy difference (in kcal/mol) of DBs with respect to the lowest energy DB.

By comparing the numbers listed in Tables 3 and 4, it might be noticed that the lowest isotropic *g*-shifts for hydroxylated (88 ppm) and aminated (215 ppm) NDs are not too distinct, but the highest ones—1113 and 582 ppm, respectively—differ much more significantly. As a consequence, their corresponding $\Delta\bar{g}$ variation ranges of 1025 and 367 ppm are not similar and, interestingly, fall in between the results of $C_{35}H_{36}$ (110 ppm) and $C_{35}F_{36}$ (1627 ppm). The total energy differences, on the other hand, are not similar either, as the highest ΔE value for hydroxylated ND is 17.2 kcal/mol [DB(O23−H23)], while the analogous value for aminated ND is almost twice as large—33.8 kcal/mol [DB(H39−N20−H40)]. In addition,

Table 4. *g*-Shifts Δg_{ii} and Their Isotropic Values $\Delta\bar{g}$ (in ppm) Calculated for DBs Introduced into Aminated Octahedral NDs of $C_{35}(NH_2)_{36}$ Size[a]

DB position	Δg_{xx}	Δg_{yy}	Δg_{zz}	$\Delta\bar{g}$	ΔE
H3−N2−H4	−188	299	533	215	31.7
H53−N27−H54	−145	342	542	246	28.8
H31−N16−H32	−143	331	572	253	30.9
H49−N25−H50	−164	356	591	261	26.2
H19−N10−H20	−196	335	686	275	27.7
H1−N1−H2	−177	419	632	291	31.3
H39−N20−H40	−137	410	665	313	33.8
H23−N12−H24	−113	426	658	324	26.8
H25−N13−H26	−131	480	693	347	17.7
H33−N17−H34	−117	529	676	363	18.7
H35−N18−H36	−89	436	747	364	28.4
H57−N29−H58	−111	516	736	380	14.7
H5−N3−H6	−52	499	723	390	28.5
H15−N8−H16	−129	501	813	395	30.9
H45−N23−H46	−105	478	858	410	29.6
H7−N4−H8	−95	562	776	414	16.6
H47−N24−H48	−44	512	789	419	18.2
H55−N28−H56	−52	520	843	437	16.3
H13−N7−H14	−86	516	927	452	7.9
H11−N6−H12	−86	516	929	453	7.9
H63−N32−H64	−128	637	918	476	6.0
H59−N30−H60	−55	650	853	483	11.2
H67−N34−H68	−135	759	833	486	
H43−N22−H44	−115	700	887	491	2.7
H41−N21−H42	−83	707	852	492	3.7
H71−N36−H72	−63	651	921	503	3.9
H21−N11−H22	−52	694	890	511	16.9
H69−N35−H70	−100	779	861	513	4.2
H17−N9−H18	−38	654	927	514	17.5
H37−N19−H38	−51	636	962	516	19.1
H65−N33−H66	−116	812	852	516	1.2
H29−N15−H30	−133	758	957	528	3.4
H51−N26−H52	−13	680	956	541	16.7
H61−N31−H62	−130	812	950	544	5.9
H9−N5−H10	7	670	970	549	15.4
H27−N14−H28	−127	803	1070	582	4.0

[a]ΔE represents the total energy difference (in kcal/mol) of DBs with respect to the lowest energy DB.

these numbers are vastly higher than those seen for $C_{35}F_{36}$ (4.45 kcal/mol), not to mention $C_{35}H_{36}$ (0.7 kcal/mol), demonstrating that some positions of DBs can be energetically very costly in $C_{35}(OH)_{36}$ and $C_{35}(NH_2)_{36}$. Regarding the lowest energy DBs, it can be noted that in both cases, they are irregular DBs, that is, OH- and NH_2-bonded C atoms, namely, DB(O35−H35) and DB(H67−N34−H68). This trend is in contrast with the one exhibited by $C_{35}H_{36}$ and $C_{35}F_{36}$ since for these systems, irregular DBs are the most energetically unfavorable. A closer look at the geometric positions of the highest energy DBs in $C_{35}(OH)_{36}$ [DB(O23−H23)] and $C_{35}(NH_2)_{36}$ [DB(H39−N20−H40)] reveals that, with respect to the structure of pure C_{35}, they are located on the geometrically equivalent C atoms. In addition, even more might be said at this point: on the basis of their geometric positions, DBs in hydroxylated and aminated NDs can be divided into the same three groups consisting of twelve DBs as in the case of hydrogenated and fluorinated NDs. However, the apparent difference is that the energies and *g*-shifts of DBs

https://doi.org/10.1021/acs.jpca.1c06253
J. Phys. Chem. A XXXX, XXX, XXX−XXX

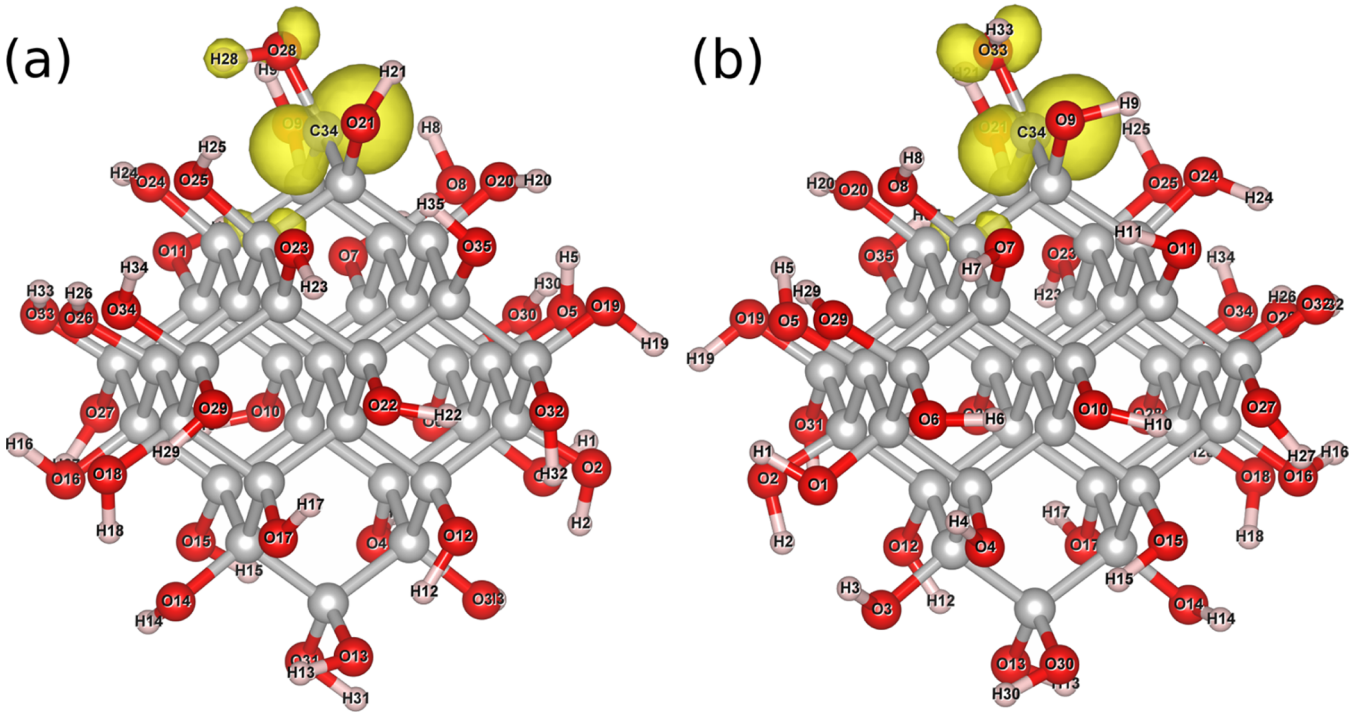

Figure 4. Spin density distribution of (a) DB(O34−H34) and (b) DB(O28−H28) introduced into $C_{35}(OH)_{36}$.

belonging to the same group are not identical—they vary within some range. In other words, although geometrically equivalent DBs do not exist in $C_{35}(OH)_{36}$ and $C_{35}(NH_2)_{36}$, geometrically similar DBs certainly do. To convincingly illustrate this from the energetic point of view, let us have a look at Table 4. Here, one may find that for some twelve DBs in $C_{35}(NH_2)_{36}$ (including the lowest energy DB), the total energy differences do not exceed 7.9 kcal/mol; for another twelve DBs, the range of ΔE is 11.2−19.1 kcal/mol, and for the last twelve DBs, the ΔE values fall within 26.2−33.8 kcal/mol. The most important part of this observation is that every DB in a particular group is located on the geometrically equivalent C atom of C_{35}, indicating that the first, second, and third groups, respectively, correspond to DB(H33/F33), DB(H28/F28), and DB(H23/F23) type of DBs met while investigating $C_{35}H_{36}$ and $C_{35}F_{36}$. The average values of $\Delta\bar{g}$ for these three groups are correspondingly equal to 503, 456, and 311 ppm. Although not so clearly expressed, the same is also true for the energetics of $C_{35}(OH)_{36}$. However, for this ND, due to a substantially larger variation range of the isotropic values of g-shifts, analogous $\Delta\bar{g}$ numbers for the aforementioned types of DBs are more distinct, as they reach 999, 425, and 160 ppm, respectively.

One more aspect that stands out when analyzing the obtained results is rather extended variation range of $\Delta\bar{g}$ for DB(H33/F33) type of DBs in the case of hydroxylated ND—from 663 ppm [DB(O34−H34)] to 1113 ppm [DB(O19−H19)]. Compared to DB(H23/F23) and DB(H28/F28) type of DBs, it is 3 times larger since the $\Delta\bar{g}$ variation range for the former group of DBs is from 88 ppm [DB(O2−H2)] to 236 ppm [DB(O1−H1)], whereas for the latter—from 351 ppm [DB(O26−H26)] to 487 ppm [DB(O10−H10)]. At the first glance, it seems that the lower bound of 663 ppm distinguishes from the rest of the numbers produced by the DB(H33/F33) type of DBs, as the next lowest value of 941 ppm [DB(O33−H33)] is only 172 ppm below the upper bound of 1113 ppm. Indeed, Figure 4 reveals that the spin density distribution of DB(O34−H34) is different from that of other DBs in the same group, represented by DB(O28−H28) since, instead of being solely on the O atom of −OH attached to C34, a part of spin density is also located on the H atom. Having in mind that DB(O34−H34) and DB(O28−H28) were introduced by removing appropriate −OH grafted to the same C atom (see Figure 3), the obvious differences in their g-shift values points to the uniqueness of all DBs present in such NDs, testifying about the need to perform calculations for every single DB these NDs possess.

Several DBs Simultaneously Present in NDs. As we have already seen, the shape of ND is an important factor that influences the g-shifts of the system. However, it is evident that shape is just one factor among many others. The question that we raise in this part of the work is related with magnetic behavior of several DBs simultaneously present in NDs. To be precise, what happens when one DB appears in the vicinity of the other?

To find this out, at first, let us take three sufficiently distant single DBs introduced into $C_{84}H_{64}$, for example, DB(H3), DB(H22), and DB(H63), as visualized in Figure 5(a)−(c), respectively. The corresponding isotropic values of their g-shifts—426, 323, and 460 ppm—are given in Table 5. In addition to these numbers, we have also provided the results calculated for several combinations of DBs simultaneously present in $C_{84}H_{64}$—the so-called multicomponent DBs. They are DB(H3 + H22), DB(H3 + H63), DB(H22 + H63), and DB(H3 + H22 + H63). Spin density visualization of the latter multicomponent DB, shown in Figure 5(d), allows us to make an assumption that the $\Delta\bar{g}$ value of this system might be taken as an arithmetic average of its components since spin density distributions of separate DBs, demonstrated in Figure 5(a)−(c), remain unaltered. In other words, the arithmetic average of $\Delta\bar{g}$ values for DB(H3), DB(H22), and DB(H63) should be approximately equal to the $\Delta\bar{g}$ value for DB(H3 + H22 + H63). We have denoted the absolute difference between these

https://doi.org/10.1021/acs.jpca.1c06253
J. Phys. Chem. A XXXX, XXX, XXX−XXX

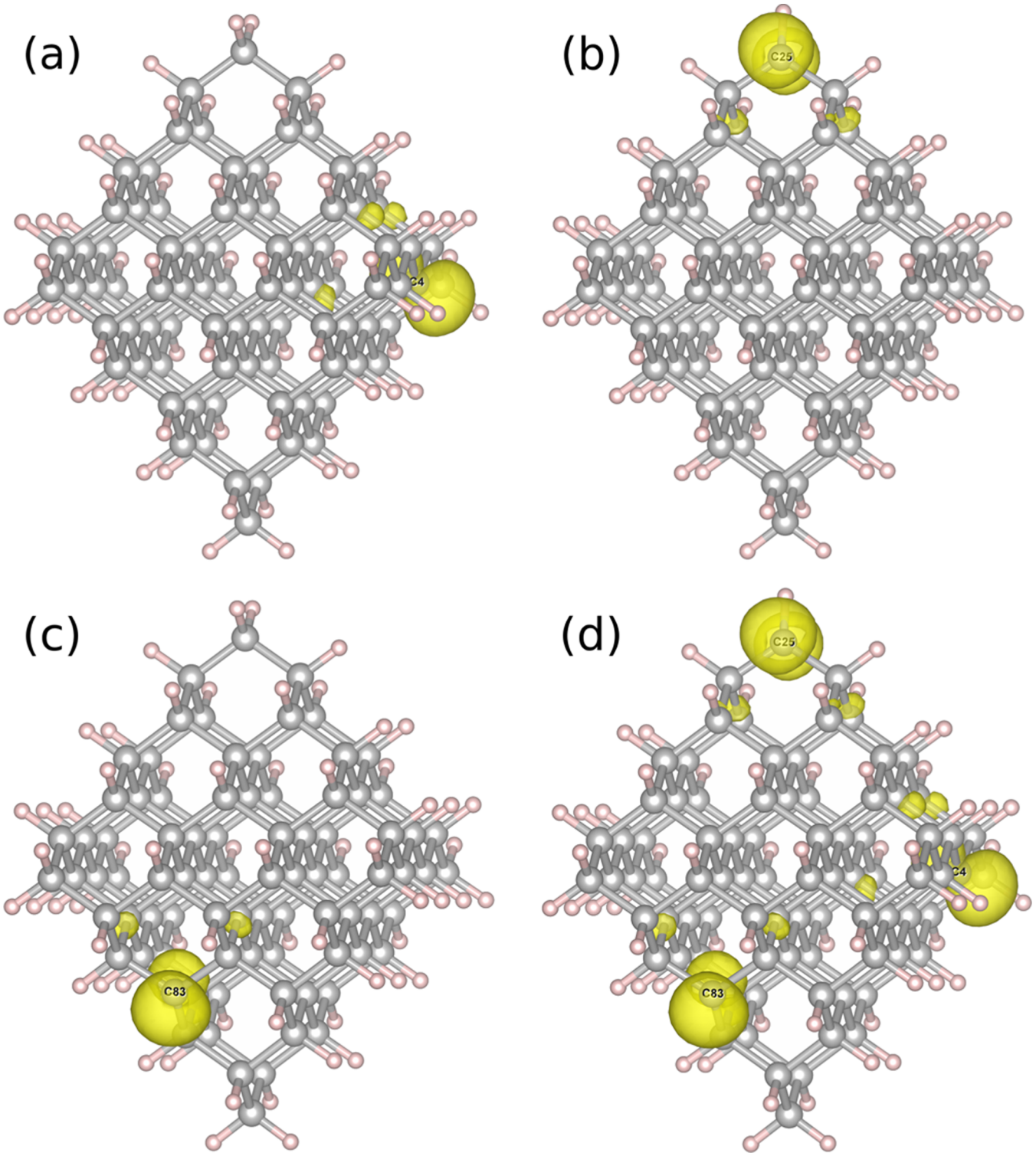

Figure 5. Spin density distribution of DBs introduced into $C_{84}H_{64}$: (a) DB(H3), (b) DB(H22), (c) DB(H63), and (d) DB(H3 + H22 + H63).

two values as $\delta\bar{g}$ and included in Table 5. Now, one can make sure that for sufficiently distant DBs, the assumption we made is valid, as $\delta\bar{g}$ for all considered multicomponent DBs is practically negligible. The analogous procedure was repeated for fluorinated NDs of the same shape and size, as visualized in Figure 6. Some of the obtained $\delta\bar{g}$ values, listed in Table 5, are slightly larger but nevertheless still very small, indicating that introduced DBs do not have any noticeable impact on each other in the case of fluorination as well. On the other hand, the situation with hydroxylated and aminated NDs would be different because geometric rearrangements on one side of such NDs can easily affect the geometry on the other, disturbing the local environments of spin densities. Therefore, only hydrogenated and fluorinated NDs are suitable for this type of investigation.

The absolute difference between $\Delta\bar{g}$ of multicomponent DB and arithmetically averaged $\Delta\bar{g}_{Av.}$ of its components, already denoted as $\delta\bar{g}$, can be used as a tool to approximately assess the

https://doi.org/10.1021/acs.jpca.1c06253
J. Phys. Chem. A XXXX, XXX, XXX−XXX

Table 5. Isotropic Values $\Delta\bar{g}$ of *g*-Shifts (in ppm) Calculated for DBs Introduced into $C_{84}H_{64}$ and $C_{84}F_{64}$[a]

ND	DB position	$\Delta\bar{g}$	$\Delta\bar{g}_{Av.}$	$\delta\bar{g}$
$C_{84}H_{64}$	H3	426		
	H22	323		
	H63	460		
	H3 + H22	377	375	2
	H3 + H63	442	443	1
	H22 + H63	391	392	1
	H3 + H22 + H63	404	403	1
$C_{84}F_{64}$	F3	530		
	F22	1689		
	F63	316		
	F3 + F22	1104	1110	6
	F3 + F63	423	423	0
	F22 + F63	1003	1003	0
	F3 + F22 + F63	842	845	3

[a] $\Delta\bar{g}_{Av.}$ represents an arithmetic average of $\Delta\bar{g}$ (in ppm) for separate DBs constituting a multicomponent DB. An absolute difference between $\Delta\bar{g}$ and $\Delta\bar{g}_{Av.}$ (in ppm) is denoted by $\delta\bar{g}$ and is evaluated as $|\Delta\bar{g} - \Delta\bar{g}_{Av.}|$.

extent to which $\Delta\bar{g}$ of the system is affected by the presence of one DB near the other. In order to establish trends inherent for hydrogenated and fluorinated NDs, we have taken $C_{35}H_{36}$ and $C_{35}F_{36}$, introduced previously investigated DBs from Tables 1 and 2, and then additionally grafted some single DBs within a distance of 3 Å, where the interaction between DBs is expected to be significant. The obtained results of *g*-tensor calculations for the examined DBs are presented in Tables 6 and 7. Here, it may be noticed that $\delta\bar{g}$ values for $C_{35}F_{36}$ are larger than those for $C_{35}H_{36}$, but overall, they are quite low, with the highest ones reaching 77 and 11 ppm, respectively. Thus, it can in principle be stated that the presence of one DB in the vicinity of the other has no substantial effect on the magnetic behavior, irrespective of the surface functionalization. In other words, the electronic structure of DBs is mostly governed by the immediate local environment in ND, and the interaction between DBs is minimal, indicating small delocalization of spin densities within ND.

Comparison to the Experiment. Unfortunately, a direct comparison between the theoretical and experimental results is not straightforward because of two essential reasons. First, different production and purification procedures applied to NDs result in differently functionalized surfaces,[35] and, unless explicitly stated as in the works of Yavkin *et al.*[36] or Panich *et al.*,[37] it is hardly possible to trace the specific surface functionalization that was present during the EPR experiment. Second, experimental measurements provide an average value of $\Delta\bar{g}$ for an ensemble of NDs that constitute a sample,[8] while our data are obtained for single nanoparticles. However, despite these issues, a few generalizations can still be made. A typical value of $\Delta\bar{g}$ for DBs of unspecified surface functionalization is ∼480 ppm, with the experimental error ranging from 100[8] to 200 ppm.[7] However, one can find more precise measurements[38] producing $\Delta\bar{g}$ of ∼500 ± 30 ppm, and we will try to compare our results to this value.

For the sake of simplicity, let us assume that the ensembles of diamond nanoparticles are formed by NDs of the same shape and size. In addition, let us make another assumption that formation of DBs occurs in a random statistical manner, which might be reasonable if one takes into account how NDs are usually obtained—by applying milling, grinding, or pulverizing techniques.[8] That said, the $\Delta\bar{g}$ values averaged over all DBs available in a particular ND are equal to 393, 416, 433, 445, 349, 528, and 424 ppm for $C_{35}H_{36}$, $C_{84}H_{64}$, $C_{165}H_{100}$, $C_{54}H_{48}$, $C_{51}H_{52}$, $C_{35}(OH)_{36}$, and $C_{35}(NH_2)_{36}$, respectively. Among these numbers, only 528 ppm of $C_{35}(OH)_{36}$ appears to agree with the experimental value, while others are slightly too low. However, it is interesting to observe that the average values of $\Delta\bar{g}$ are quite similar for all the three aforementioned functionalization schemes, despite the fact that the hydroxylated ND exhibits a much larger variation range of $\Delta\bar{g}$.

Fluorinated NDs, intentionally not included in our previous analysis, deserve exceptional attention, as one may find EPR experiment dedicated for this type of surface functionalization.[37] The measured $\Delta\bar{g}$ value for DBs is ∼380 ± 200 ppm, and it turns out to be lower than the average $\Delta\bar{g}$ we have evaluated for $C_{35}F_{36}$, $C_{84}F_{64}$, $C_{165}F_{100}$, $C_{54}F_{48}$, and $C_{51}F_{52}$: 715, 646, 642, 614, and 1481 ppm, correspondingly. Among these values, 614 ppm of cubic ND shows the closest resemblance to the upper bound of experimental result (∼580 ppm), whereas octahedral NDs get closer to this bound with an increase in their size. Tetrahedral ND, on the other hand, demonstrates a huge discrepancy, with its average $\Delta\bar{g}$ value of 1481 ppm more than twice overestimating the experimental findings. Although the shape of NDs might be quite irregular,[7] tetrahedral approximation seems to be definitely unfavorable, at least for the selected size of NDs with fluorinated surface.

It should be noted, though, that our assumption on formation of DBs in a random statistical manner does not take into account the differences of total energies between distinct DBs. In order to find out the influence of this factor, we have evaluated formation probabilities of DBs *via* Boltzmann distribution at a temperature of 300 K and applied them while estimating the average value of $\Delta\bar{g}$ for a particular ND. Hence, the resulting Boltzmann-weighted average values of isotropic *g*-shifts are equal to 412, 431, 444, 488, 397, 1045, and 490 ppm for $C_{35}H_{36}$, $C_{84}H_{64}$, $C_{165}H_{100}$, $C_{54}H_{48}$, $C_{51}H_{52}$, $C_{35}(OH)_{36}$, and $C_{35}(NH_2)_{36}$, respectively. Compared to the previous analysis, hydrogenated NDs demonstrate very similar numbers, and it should not be particularly surprising, as the $\Delta\bar{g}$ values of their DBs fall in a rather narrow range and the formation probabilities are quite evenly distributed. However, the situation is totally different regarding aminated and hydroxylated NDs, although it is not apparently reflected in the average isotropic *g*-shift of the former (one may notice only a slight increase from 424 to 490 ppm). The point is that for $C_{35}(NH_2)_{36}$ and $C_{35}(OH)_{36}$, the dominant contribution to the average $\Delta\bar{g}$ value is given by the lowest energy DB (87 and 77%, respectively), indicating that the hydroxylated ND now exhibits a much higher number of 1045 ppm in comparison to the previously obtained 528 ppm. In the context of typical experimental findings (∼480 ± 200 ppm), this value definitely stands out, raising an intriguing question what sort of results one should expect if measurements were performed for NDs solely functionalized with the OH group.

Speaking about fluorinated NDs, their situation remains that of $C_{35}(NH_2)_{36}$ and $C_{35}(OH)_{36}$ since one or at most two types of DBs in principle determine the average value of $\Delta\bar{g}$. The numbers evaluated by applying Boltzmann distribution are equal to 426, 565, 705, 148, and 816 ppm for $C_{35}F_{36}$, $C_{84}F_{64}$, $C_{165}F_{100}$, $C_{54}F_{48}$, and $C_{51}F_{52}$, correspondingly. Here, one may find an interesting trend that with an increase in their size, octahedral NDs exhibit an increase in their average $\Delta\bar{g}$ values,

https://doi.org/10.1021/acs.jpca.1c06253
J. Phys. Chem. A XXXX, XXX, XXX−XXX

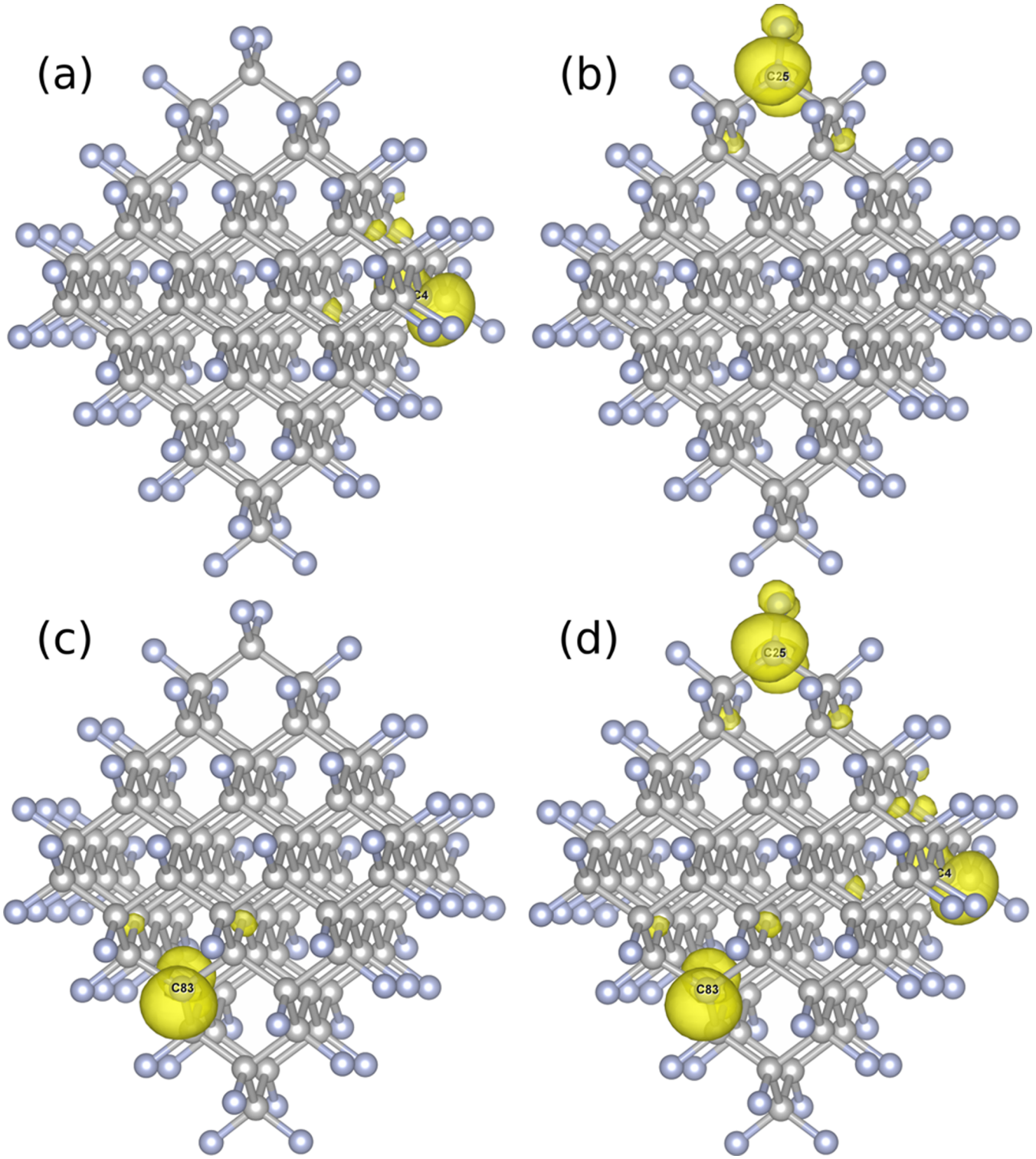

Figure 6. Spin density distribution of DBs introduced into $C_{84}F_{64}$: (a) DB(F3), (b) DB(F22), (c) DB(F63), and (d) DB(F3 + F22 + F63).

finally exceeding the upper bound of the experiment (~580 ppm). This bound is also exceeded by tetrahedral NDs in agreement with previous analysis. However, the result of cubic ND is very close to the lower bound of the experiment (~180 ppm), which appears to be the opposite to what we have obtained before when $\Delta\overline{g}$ was not too far from the upper bound.

In order to facilitate the analysis and interpretation of experimental spectra registered during, for example, the electron-nuclear double-resonance measurements, we have also computed ^{13}C isotropic hyperfine coupling constants for DBs in $C_{35}H_{36}$, $C_{35}F_{36}$, $C_{35}(OH)_{36}$, and $C_{35}(NH_2)_{36}$. The calculated constants vary in the ranges of 109−196 MHz for hydrogenated NDs, 228−245 MHz for fluorinated NDs, 152−206 MHz for hydroxylated NDs, and 90−187 MHz for aminated NDs. The respective average values are 165, 235, 185, and 154 MHz if one makes an assumption that formation of DBs occurs in a random statistical manner, while the

https://doi.org/10.1021/acs.jpca.1c06253
J. Phys. Chem. A XXXX, XXX, XXX−XXX

Table 6. Isotropic Values $\Delta\bar{g}$ of *g*-Shifts (in ppm) Calculated for DBs Introduced into $C_{35}H_{36}$[a]

DB position	$\Delta\bar{g}$	$\Delta\bar{g}_{Av.}$	$\delta\bar{g}$
H23 + H25	442	436	6
H23 + H29	423	426	3
H28 + H8	423	426	3
H28 + H29	420	416	4
H28 + H31	381	371	10
H28 + H32	379	371	8
H33 + H24	382	371	11
H33 + H28	379	371	8

[a] $\Delta\bar{g}_{Av.}$ represents an arithmetic average of $\Delta\bar{g}$ (in ppm) for separate DBs constituting a multicomponent DB. An absolute difference between $\Delta\bar{g}$ and $\Delta\bar{g}_{Av.}$ (in ppm) is denoted by $\delta\bar{g}$ and is evaluated as $|\Delta\bar{g} - \Delta\bar{g}_{Av.}|$.

Table 7. Isotropic Values $\Delta\bar{g}$ of *g*-Shifts (in ppm) Calculated for DBs Introduced into $C_{35}F_{36}$[a]

DB position	$\Delta\bar{g}$	$\Delta\bar{g}_{Av.}$	$\delta\bar{g}$
F23 + F25	26	46	20
F23 + F29	302	236	66
F28 + F8	302	236	66
F28 + F29	374	427	53
F28 + F31	973	1050	77
F28 + F32	983	1050	67
F33 + F24	973	1050	77
F33 + F28	984	1050	66

[a] $\Delta\bar{g}_{Av.}$ represents an arithmetic average of $\Delta\bar{g}$ (in ppm) for separate DBs constituting a multicomponent DB. An absolute difference between $\Delta\bar{g}$ and $\Delta\bar{g}_{Av.}$ (in ppm) is denoted by $\delta\bar{g}$ and is evaluated as $|\Delta\bar{g} - \Delta\bar{g}_{Av.}|$.

application of Boltzmann distribution results in 178, 232, 167, and 116 MHz, correspondingly. It should also be mentioned that the provided isotropic hyperfine coupling constants are for those ^{13}C atoms that possess the dominant part of spin density, as the calculated values for the neighboring ^{13}C atoms are much lower.

CONCLUSIONS

In this work, the electronic *g*-tensor calculations were carried out for DBs introduced into NDs that underwent four different surface functionalizations—hydrogenation, fluorination, hydroxylation, and amination. For hydrogenated and fluorinated NDs, it is shown that the variation range of *g*-shifts is much larger for the latter, as are the total energy differences between the highest and the lowest energy DBs within the same ND. Such findings indicate that, compared to the local environment created by H atoms, the local environment created by F atoms has a much more pronounced influence on the magnetic behavior as well as energetics of the investigated systems. Moreover, the distinction between these two geometrically identical functionalization schemes manifests in such a way that geometric positions of the lowest energy DBs in hydrogenated NDs do not match the geometric positions of the lowest energy DBs in fluorinated NDs. On the other hand, for octahedral NDs, the highest energy DBs coincide, and it is interesting to note that these DBs are irregular, that is, formed by H- and F-bonded dangling C atoms. On the whole, it is found that the shape—tested by octahedral, cubic, and tetrahedral NDs—is an important factor significantly affecting the energetics and *g*-shifts of DBs, while the impact of the size—tested by octahedral C_{35}-, C_{84}-, and C_{165}-sized systems—is much less expressed.

Regarding hydroxylated and aminated NDs, it is revealed that although geometrically identical DBs do not exist in either $C_{35}(OH)_{36}$ or $C_{35}(NH_2)_{36}$, geometrically similar DBs do, and they can be divided into the same groups as in the case of $C_{35}H_{36}$ or $C_{35}F_{36}$. However, the apparent difference is that the energies and *g*-shifts of DBs belonging to the same group are no longer identical—they exhibit a variation of some range. Another feature that stands out is the lowest energy DBs, which are irregular, that is, formed by OH- and NH_2-bonded C atoms. It contrasts with hydrogenated and fluorinated NDs of the same octahedral shape, where irregular DBs are the least energetically favorable. The variation range of *g*-shifts is larger for hydroxylated than for aminated ND, whereas the opposite is seen for the total energy differences. Overall, the latter numbers are rather high, demonstrating that some positions of DBs can be energetically very costly in $C_{35}(OH)_{36}$ and $C_{35}(NH_2)_{36}$.

Additionally, the simultaneous presence of several DBs in hydrogenated and fluorinated NDs was analyzed, which allowed us to conclude that the presence of one DB in the vicinity of the other has no substantial effect on the magnetic behavior, irrespective of the surface functionalization. Concerning a comparison to the typical EPR experiment performed for NDs of unspecified surface functionalization, it is shown that the average values of isotropic *g*-shifts evaluated for hydrogenated and aminated NDs agree with the experimental data within the margins of error. However, the situation is quite different for hydroxylated NDs since the average isotropic *g*-shift obtained by applying Boltzmann distribution clearly disagrees with the experiment. The same is also true for tetrahedral ND in the case of fluorination, as its average isotropic *g*-shift is significantly higher than experimental findings.

AUTHOR INFORMATION

Corresponding Author

Šarūnas Masys − *Institute of Theoretical Physics and Astronomy, Faculty of Physics, Vilnius University, LT-10257 Vilnius, Lithuania;* orcid.org/0000-0003-0004-1104; Email: sarunas.masys@tfai.vu.lt

Authors

Valdas Jonauskas − *Institute of Theoretical Physics and Astronomy, Faculty of Physics, Vilnius University, LT-10257 Vilnius, Lithuania*

Zilvinas Rinkevicius − *Department of Theoretical Chemistry & Biology, School of Engineering Sciences in Chemistry, Biotechnology and Health, KTH Royal Institute of Technology, SE-10691 Stockholm, Sweden; Department of Physics, Faculty of Mathematics and Natural Sciences, Kaunas University of Technology, LT-51368 Kaunas, Lithuania;* orcid.org/0000-0003-2729-0290

Complete contact information is available at: https://pubs.acs.org/10.1021/acs.jpca.1c06253

Notes

The authors declare no competing financial interest.

ACKNOWLEDGMENTS

The authors are thankful for the HPC resources provided by the IT Research Center of Vilnius University.

https://doi.org/10.1021/acs.jpca.1c06253
J. Phys. Chem. A XXXX, XXX, XXX−XXX

REFERENCES

(1) Rej, E.; Gaebel, T.; Boele, T.; Waddington, D. E. J.; Reilly, D. J. Hyperpolarized nanodiamond with long spin-relaxation times. *Nat. Commun.* **2015**, *6*, 8459.

(2) Tinwala, H.; Wairkar, S. Production, surface modification and biomedical applications of nanodiamonds: A sparkling tool for theranostics. *Mater. Sci. Eng., C* **2019**, *97*, 913−931.

(3) Lai, H.; Stenzel, M. H.; Xiao, P. Surface engineering and applications of nanodiamonds in cancer treatment and imaging. *Int. Mater. Rev.* **2020**, *65*, 189−225.

(4) Wang, E. C.; Wang, A. Z. Nanoparticles and their applications in cell and molecular biology. *Integr. Biol.* **2013**, *6*, 9−26.

(5) Waddington, D. E. J.; Boele, T.; Rej, E.; McCamey, D. R.; King, N. J. C.; Gaebel, T.; Reilly, D. J. Phase-encoded hyperpolarized nanodiamond for magnetic resonance imaging. *Sci. Rep.* **2019**, *9*, 5950.

(6) Waddington, D. E. J.; Sarracanie, M.; Zhang, H.; Salameh, N.; Glenn, D. R.; Rej, E.; Gaebel, T.; Boele, T.; Walsworth, R. L.; Reilly, D. J.; et al. Nanodiamond-enhanced MRI via in situ hyperpolarization. *Nat. Commun.* **2017**, *8*, 15118.

(7) Panich, A. M.; Sergeev, N. A.; Shames, A. I.; Osipov, V. Y.; Boudou, J.-P.; Goren, S. D. Size dependence of ^{13}C nuclear spin-lattice relaxation in micro- and nanodiamonds. *J. Phys.: Condens. Matter* **2015**, *27*, 072203.

(8) Shames, A. I.; Panich, A. M. *Nanodiamonds: Advanced Material Analysis, Properties and Applications*; Arnault, J.-C., Ed.; Elsevier: Amsterdam, 2017; pp 131−154.

(9) Rinkevicius, Z.; de Almeida, K. J.; Vahtras, O. Density functional restricted-unrestricted approach for nonlinear properties: Application to electron paramagnetic resonance parameters of square planar copper complexes. *J. Chem. Phys.* **2008**, *129*, 064109.

(10) Chipaux, M.; van der Laan, K. J.; Hemelaar, S. R.; Hasani, M.; Zheng, T.; Schirhagl, R. Nanodiamonds and their applications in cells. *Small* **2018**, *14*, 1704263.

(11) Kratochvílová, I.; Šebera, J.; Ashcheulov, P.; Golan, M.; Ledvina, M.; Míčová, J.; Mravec, F.; Kovalenko, A.; Zverev, D.; Yavkin, B.; et al. Magnetical and optical properties of nanodiamonds can be tuned by particles surface chemistry: Theoretical and experimental study. *J. Phys. Chem. C* **2014**, *118*, 25245−25252.

(12) Masys, Š.; Rinkevicius, Z.; Tamulienė, J. Electronic g-tensors of nanodiamonds: Dependence on the size, shape, and surface functionalization. *J. Chem. Phys.* **2019**, *151*, 144305.

(13) Barnard, A. S. Modeling polydispersive ensembles of diamond nanoparticles. *Nanotechnology* **2013**, *24*, 085703.

(14) Neese, F. The ORCA program system. *Wiley Interdiscip. Rev.: Comput. Mol. Sci.* **2012**, *2*, 73−78.

(15) Neese, F. Software update: The ORCA program system, version 4.0. *Wiley Interdiscip. Rev.: Comput. Mol. Sci.* **2018**, *8*, No. e1327.

(16) Grimme, S.; Brandenburg, J. G.; Bannwarth, C.; Hansen, A. Consistent structures and interactions by density functional theory with small atomic orbital basis sets. *J. Chem. Phys.* **2015**, *143*, 054107.

(17) Masys, Š.; Rinkevicius, Z.; Tamulienė, J. Computational study on the electronic g-tensors of hydrophilic and hydrophobic nanodiamonds interacting with water. *J. Chem. Phys.* **2020**, *152*, 144302.

(18) Becke, A. D. Density-functional thermochemistry. III. The role of exact exchange. *J. Chem. Phys.* **1993**, *98*, 5648−5652.

(19) Stephens, P. J.; Devlin, F. J.; Chabalowski, C. F.; Frisch, M. J. Ab initio calculation of vibrational absorption and circular dichroism spectra using density functional force fields. *J. Phys. Chem.* **1994**, *98*, 11623−11627.

(20) Krishnan, R.; Binkley, J. S.; Seeger, R.; Pople, J. A. Self-consistent molecular orbital methods. XX. A basis set for correlated wave functions. *J. Chem. Phys.* **1980**, *72*, 650−654.

(21) Frisch, M. J.; Pople, J. A.; Binkley, J. S. Self-consistent molecular orbital methods 25. Supplementary functions for Gaussian basis sets. *J. Chem. Phys.* **1984**, *80*, 3265−3269.

(22) Masys, Š.; Rinkevicius, Z.; Tamulienė, J. On the magnetic properties of nanodiamonds: Electronic g-tensor calculations. *J. Chem. Phys.* **2019**, *151*, 044305.

(23) Neese, F. An improvement of the resolution of the identity approximation for the formation of the Coulomb matrix. *J. Comput. Chem.* **2003**, *24*, 1740−1747.

(24) Neese, F.; Wennmohs, F.; Hansen, A.; Becker, U. Efficient, approximate and parallel Hartree-Fock and hybrid DFT calculations. A 'chain-of-spheres' algorithm for the Hartree-Fock exchange. *Chem. Phys.* **2009**, *356*, 98−109.

(25) Stoychev, G. L.; Auer, A. A.; Neese, F. Automatic generation of auxiliary basis sets. *J. Chem. Theory Comput.* **2017**, *13*, 554−562.

(26) Koseki, S.; Schmidt, M. W.; Gordon, M. S. MCSCF/6-31G(d,p) calculations of one-electron spin-orbit coupling constants in diatomic molecules. *J. Phys. Chem.* **1992**, *96*, 10768−10772.

(27) Koseki, S.; Gordon, M. S.; Schmidt, M. W.; Matsunaga, N. Main group effective nuclear charges for spin-orbit calculations. *J. Phys. Chem.* **1995**, *99*, 12764−12772.

(28) Koseki, S.; Schmidt, M. W.; Gordon, M. S. Effective nuclear charges for the first- through third-row transition metal elements in spin-orbit calculations. *J. Phys. Chem. A* **1998**, *102*, 10430−10435.

(29) Weigend, F. Accurate Coulomb-fitting basis sets for H to Rn. *Phys. Chem. Chem. Phys.* **2006**, *8*, 1057−1065.

(30) Kruse, H.; Grimme, S. A geometrical correction for the inter- and intra-molecular basis set superposition error in Hartree-Fock and density functional theory calculations for large systems. *J. Chem. Phys.* **2012**, *136*, 154101.

(31) Grimme, S.; Antony, J.; Ehrlich, S.; Krieg, H. A consistent and accurate ab initio parametrization of density functional dispersion correction (DFT-D) for the 94 elements H-Pu. *J. Chem. Phys.* **2010**, *132*, 154104.

(32) Grimme, S.; Ehrlich, S.; Goerigk, L. Effect of the damping function in dispersion corrected density functional theory. *J. Comput. Chem.* **2011**, *32*, 1456−1465.

(33) Barone, V. *Recent Advances in Density Functional Methods*; Chong, D. P., Ed.; World Scientific: Singapore, 1995; pp 287−334.

(34) Momma, K.; Izumi, F. VESTA3 for three-dimensional visualization of crystal, volumetric and morphology data. *J. Appl. Crystallogr.* **2011**, *44*, 1272−1276.

(35) Krueger, A.; Lang, D. Functionality is key: Recent progress in the surface modification of nanodiamond. *Adv. Funct. Mater.* **2012**, *22*, 890−906.

(36) Yavkin, B. V.; Zverev, D. G.; Mamin, G. V.; Gafurov, M. R.; Orlinskii, S. B. Influence of the chemical modification of the nanodiamond surface on electron paramagnetic resonance/electron-nuclear double resonance spectra of intrinsic nitrogen defects. *J. Phys. Chem. C* **2019**, *123*, 22384−22389.

(37) Panich, A. M.; Vieth, H.-M.; Shames, A. I.; Froumin, N.; Ôsawa, E.; Yao, A. Structure and bonding in fluorinated nanodiamond. *J. Phys. Chem. C* **2010**, *114*, 774−782.

(38) Shames, A. I.; Panich, A. M.; Kempiński, W.; Alexenskii, A. E.; Baidakova, M. V.; Dideikin, A. T.; Osipov, V. Y.; Siklitski, V. I.; Osawa, E.; Ozawa, M.; et al. Defects and impurities in nanodiamonds: EPR, NMR and TEM study. *J. Phys. Chem. Solids* **2002**, *63*, 1993−2001.

https://doi.org/10.1021/acs.jpca.1c06253
J. Phys. Chem. A XXXX, XXX, XXX−XXX